2020 IEEE/RSJ International Conference on Intelligent Robots and Systems (IROS)
October 25-29, 2020, Las Vegas, NV, USA (Virtual)

FreeBOT: A Freeform Modular Self-reconfigurable Robot with Arbitrary Connection Point - Design and Implementation

Guanqi Liang[1,2], Haobo Luo[1,2], Ming Li[1,2], Huihuan Qian[1,2], and Tin Lun Lam[1,2,†]

***Abstract*— This paper proposes a novel modular self-reconfigurable robot (MSRR) "FreeBOT", which can be connected freely at any point on other robots. FreeBOT is mainly composed of two parts: a spherical ferromagnetic shell and an internal magnet. The connection between the modules is genderless and instant, since the internal magnet can freely attract other FreeBOT spherical ferromagnetic shells, and not need to be precisely aligned with the specified connector. This connection method has fewer physical constraints, so the FreeBOT system can be extended to more configurations to meet more functional requirements. FreeBOT can accomplish multiple tasks although it only has two motors: module independent movement, connector management and system reconfiguration. FreeBOT can move independently on the plane, and even climb on ferromagnetic walls; a group of FreeBOTs can traverse complex terrain. Numerous experiments have been conducted to test its function, which shows that the FreeBOT system has great potential to realize a freeform robotic system.**

Fig. 1. A freeform MSRR system - FreeBOT

I. Introduction

Modular self-reconfigurable robots (MSRR) have become a hot research topic in recent years [1]–[9]. MSRR system consists of many repeated modules, which can rearrange themselves into different configurations according to task requirements. The previous MSRR modules are difficult to realize a freeform robotic systems because they have lots of physical constraints such as: the module connectors are gender-opposite and discrete; the modules need to plan trajectories to align the connectors while self-assembly; the connection between modules is time-consuming and has a low success rate.

Through the docking mechanism, the MSRR can realize the connection/separation and system reconfiguration between modules. Therefore, the docking mechanism is one of the most basic components of the MSRR system and many creative docking mechanisms have been designed. For example, the hooks that are activated by DC motors [1], [5], [10]–[12], permanent magnets [2], electromagnets [13], or electro-permanent magnets [14]. In [15], the author proposed the concept of "the area of acceptance" for MSRR, which is defined as "the range of possible starting conditions for which mating will be successful"; a connector with a larger area of acceptance has a higher success rate when connecting. The hooks activated by DC motor allow the modules to be strongly connected, but has a small acceptance area and needs accurate alignment, which requires the module units to plan the trajectory when connecting [10]. It is not an efficient connection mechanism for the MSRR system. Connections between magnets or electromagnets can increase the acceptance area [2], [14] since an accurate alignment is not required. When two MSRR modules with paired magnets (or paired electromagnets) approach, they are automatically combined together under a magnetic field. However, the previous connections between magnets or electromagnets must be gender-opposed; it will increase some path planning constraints for the connection between modules [3], [4], [16]. Since the configuration of the previous MSRR system is restricted by the location and gender of the connector, it has become a growing consensus to equip the MSRR module with multiple connectors. If one module can be connected to multiple modules at the same time, the configuration of the MSRR system will be enriched to meet more functional requirements. However, the module with multiple connectors not only increases the weight, volume and manufacturing cost of the robot, but also brings complex physical constraints for path planning at the algorithm level. Therefore, it is still challenging to design an effective and freeform MSRR module.

This paper proposes a novel MSRR called FreeBOT (Freeform Robot), which can be connected together flexibly in an effective way with fewer physical constraints (as shown in Fig. 1). FreeBOT has the same basic functions as the most advanced MSRR: modules can move independently, modules can be connected/separated without manual assistance, and system configurations can be rearranged. In addition, The connection between modules is genderless and instant, since the internal magnet can freely attract other

*This paper is partially supported by funding 2019-INT008 from the Shenzhen Institute of Artificial Intelligence and Robotics for Society.

[1]The Chinese University of Hong Kong, Shenzhen.
[2]The Shenzhen Institute of Artificial Intelligence and Robotics for Society.
[†]Corresponding author is Tin Lun Lam tllam@cuhk.edu.cn

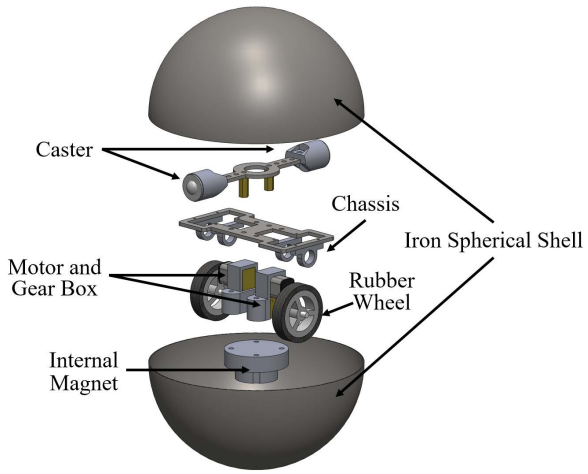

Fig. 2. Assembly exploded diagram of FreeBOT

FreeBOT spherical ferromagnetic shells, and not need to be precisely aligned with the specified connector. When it comes to motion performance, a FreeBOT can travel along planar surfaces, and even climb ferromagnetic slopes or walls; a group of FreeBOTs can be rearranged into different configurations to travel through more complicated terrain. Since this connection has fewer physical constraints, the FreeBOT system can be extended to more configurations to meet more functional requirements, which has great potential to realize a freeform robotic system.

This paper is organized as follows. Section II describes the mechanical design. The motion of FreeBOT and experiment results are introduced in Section III and IV respectively. Section V compares FreeBOT with state-of-the-art MSRRs. Finally, conclusions and future work are given in Section VI.

II. Mechanical Design

A. FreeBOT design

Fig. 2 is the assembly exploded diagram of the FreeBOT. FreeBOT is a spherical robot equipped with internal magnets, which is mainly composed of two parts: a ferromagnetic spherical shell and an internal driving mechanism. The internal driving mechanism is a vehicle equipped with two rubber wheels, which are driven by two DC motors through gearboxes. A strong permanent magnet is installed at the bottom of the internal vehicle, and the ferromagnetic spherical shell is made of iron, so the internal vehicle will always adhere to the spherical shell due to the great attraction caused between them. It is a non-touch connection between the magnet and the inner surface of the spherical shell, since the internal vehicle only touch the inner surface through the rubber wheel, the magnet and the spherical iron shell are not in physical contact, so the magnet is easy to move in the spherical shell. Two casters are placed in front and in rear of the internal vehicle through a strip-shaped aluminum alloy plate to ensure that the internal vehicle remains balanced in the spherical shell. The gravity of FreeBOT can be changed through changing the position of the internal vehicle in the spherical shell by controlling two DC motors, so that FreeBOT rolling on the plane can be realized. Due to

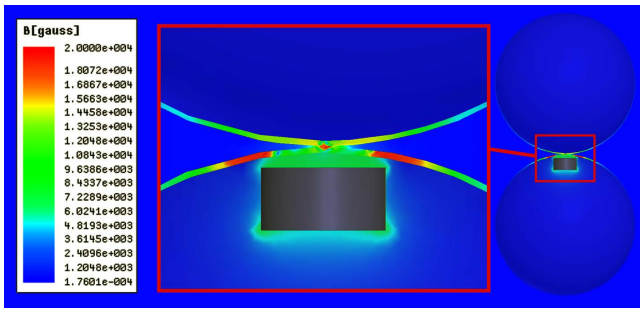

Fig. 3. Magnetic field excited by the internal magnet

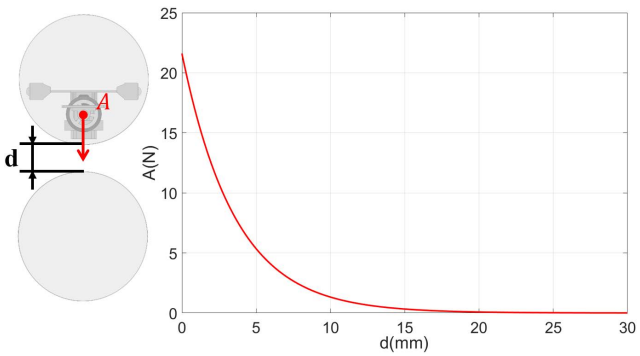

Fig. 4. Magnetic attraction versus distance between two FreeBOTs

the powerful internal magnet, a single FreeBOT can move on the slot, even on the vertical ferromagnetic surface. In addition, the position of the internal magnet in the spherical shell depends on the position of the internal vehicle, this makes a freeform connection become possible, which will be discussed in Section III.

B. Connector

A novel connection method is adopted in FreeBOT system: FreeBOT is equipped with static permanent magnets, so that the magnetic field can be transmitted to the outside; the shell will be magnetized when approaching the magnetic field, since FreeBOT's ferromagnetic spherical shell is made of iron, therefore, when a FreeBOT approaches the internal magnet of another FreeBOT, the magnetic attraction is generated. Since the size of the internal magnet is small, but the magnetic field strength is large (the size of the magnet is $20mm \times 10mm \times 10mm$, but the magnetic remanence is $14700\ gauss$), so it can excite a small but strong external magnetic field. Fig. 3 shows the magnetic field distribution when one FreeBOT attracts another FreeBOT (ANSYS is adopted to analyze the magnetic field of the FreeBOT). We can see that the internal magnet excites a magnetic field, which penetrates through the shell and transmits to the outside, and the two spherical shells are magnetized by this internal magnet. Fig. 4 shows the variation of magnetic force with the distance between two FreeBOTs. When $d = 0$, the magnetic force reaches its maximum value of $22.6N$. With the increase of distance, the magnetic force decreases exponentially.

Fig. 5 shows the attraction of the internal magnet to other spherical shells when it moves, and the magnetic attraction is divided into two directions, parallel and perpendicular. For

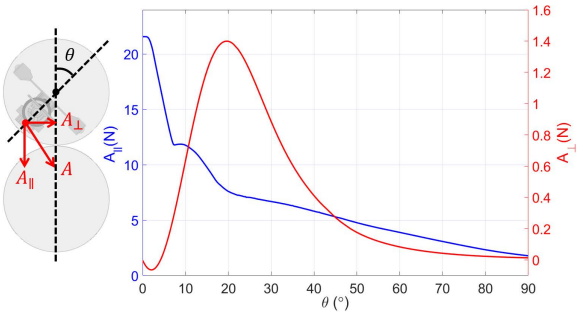

Fig. 5. Magnetic attraction versus lifting angle

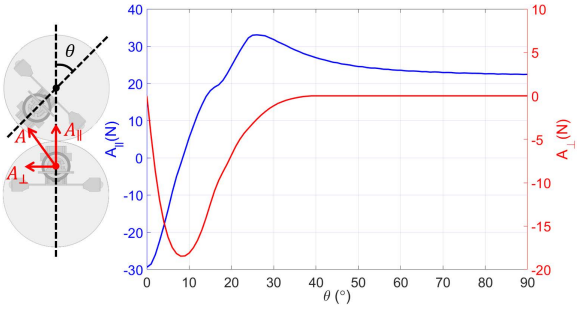

Fig. 6. Magnetic attraction versus lifting angle when two magnets are close

the parallel direction, the magnetic attractive force decreases as θ increases. We can see that $A_{\parallel}$ is always positive, which means that as long as $\theta > 0°$, there will always be a force pointing from the internal magnet to other FreeBOT. For the perpendicular direction, as θ increases, $A_{\perp}$ first decreases and then increases, and the maximum value is only $1.4N$. During changing the position of the internal magnet, $A_{\parallel}$ is much larger than $A_{\perp}$. Therefore, we can choose a suitable θ to realize the reconfiguration of a FreeBOT on another FreeBOT surface.

The above analysis shows that which small area of the spherical iron shell will attract other FreeBOT depends on the position of the internal magnet. However, when the two internal magnets are close together, the case is different. Fig. 6 shows the forces of two internal magnets that are closed, and we decompose the magnetic attraction into parallel and perpendicular directions similarly. For the parallel direction, when $0° < \theta < 8°$, $A_{\parallel}$ is negative; when $\theta > 8°$, $A_{\parallel}$ becomes positive. $A_{\parallel}$ will increase with the increase of θ, and finally stabilize at $22.6N$ (it is also the maximum attractive force in Fig. 4). This means that the two internal magnets repel each other when they are very close and the attraction of the internal magnet to other FreeBOT will return to normal once the two internal magnets are far away. For the perpendicular direction, $A_{\perp}$ is always negative, which means that they are mutually exclusive. When θ is small, there will be a large repulsive force in the perpendicular direction, but when θ is large, the repulsive force will disappear. In general, since the two internal magnets are of the same gender, the two FreeBOTs will repel each other when their internal magnets face each other.

In summary, FreeBOT's internal magnet can be connected to the entire spherical shell of other FreeBOT. The location

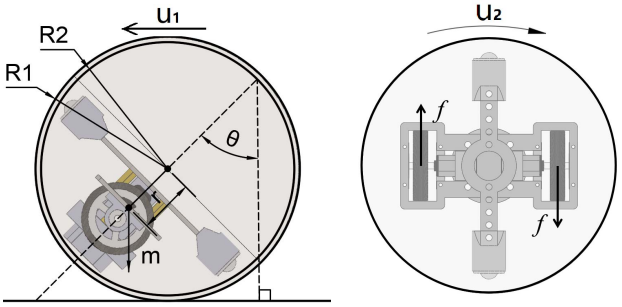

(a) Side view when rolling (b) Top view when turning

Fig. 7. Motion of FreeBOT

of the internal magnet is the only blind spot for connection. It is encouraging that this is a genderless connector since the two FreeBOTs are essentially connected by their spherical iron shell, and the connection of two FreeBOTs can be at almost any point on their spherical iron shell. Therefore, as long as two FreeBOTs touch each other, we can control the internal vehicle to realize their connection. Based on this design, FreeBOT can achieve some interesting motions.

III. Motion of FreeBOT

A. Module Independent Motion

FreeBOT is essentially a spherical robot, so the general movement method of spherical robots is also applicable to FreeBOT. Fig. 7(a) shows the side view of a FreeBOT during rolling. When the two driving wheels rotate in the same direction, the internal vehicle moves along the inner surface of the spherical shell, and then the gravity center of FreeBOT is raised and torque is provided to make FreeBOT roll forward. The driving torque τ is given by

$$\tau = rmsin\theta = I\alpha, \tag{1}$$

where r is the distance from the sphere center to the gravity center of the internal body, m is the mass of the internal driving mechanism, θ is the rolling angle of the sphere, I is the inertial moment of the spherical shell and α is the angular acceleration of the FreeBOT.

Assuming the spherical shell material is homogeneous, the inertial moment of the spherical shell is

$$I = \frac{2}{5} m_{ball} \frac{R_1^5 - R_2^5}{R_1^3 - R_2^3} + \frac{m_{ball}}{4}(R_1 + R_2)^2, \tag{2}$$

where m_{ball} is the mass of the spherical shell, R_1 is the external radius of the shell, and R_2 is the internal radius of the shell.

The angular acceleration α is denoted as

$$\alpha = \frac{rmsin\theta}{I} = Kr\frac{m}{m_{ball}}sin\theta, \tag{3}$$

where

$$K = \left(\frac{2}{5} \cdot \frac{R_1^5 - R_2^5}{R_1^3 - R_2^3} + \frac{(R_1 + R_2)^2}{4}\right)^{-1}.$$

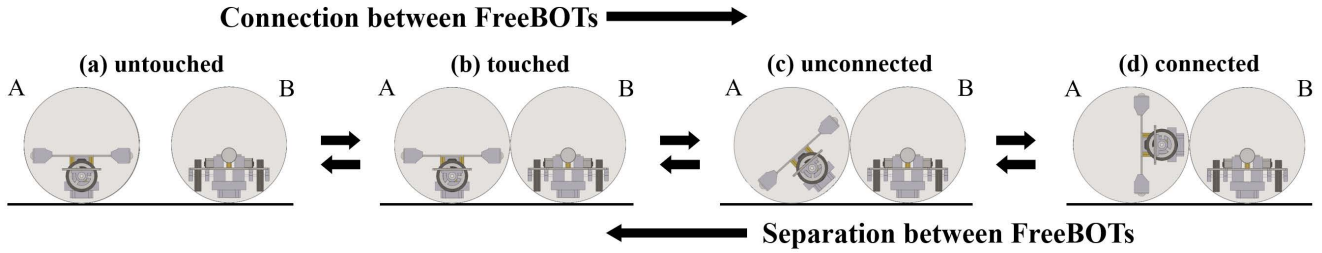

Fig. 8. Connection and separation between FreeBOTs

The coefficient K depends on the geometry, so for a FreeBOT with given structure and mass, the rolling velocity only depends on the rolling angle of the internal vehicle.

Fig. 7(b) shows the top view of a FreeBOT during turning. When two motors rotate in different directions, the friction from the iron shell will produce a torque around the central axis of the internal vehicle. The internal vehicle will rotate around the axis to change the orientation.

Bicchi [17] introduces a kinematic model for general spherical robot. It is found that this model is also suitable to represent the properties of the FreeBOT moving on the flat ground. According to [17], the kinematics in our notations and coordinate system can be formulated as:

$$\begin{bmatrix} \dot{x} \\ \dot{y} \\ \dot{\phi} \\ \dot{\beta} \\ \dot{\psi} \\ \dot{\theta} \end{bmatrix} = \begin{bmatrix} \cos\theta \\ \sin\theta \\ \frac{\sin(\psi-\theta)}{R\cos\beta} \\ \frac{\cos(\psi-\theta)}{R} \\ \frac{\tan\beta\sin(\psi-\theta)}{R} \\ 0 \end{bmatrix} u_1 + \begin{bmatrix} 0 \\ 0 \\ 0 \\ 0 \\ 0 \\ 1 \end{bmatrix} u_2, \tag{4}$$

where $(x, y, \phi, \beta, \psi, \theta)^T$ denote the configuration of the robot, parameterized by the xy location of the sphere center, the ZYX Euler angles, ϕ, β, ψ, and the steering angle of the internal driving mechanism with respect to the FreeBOT body, θ, u_1 is forward speed, and u_2 is the steering speed.

B. Connection and separation

Fig. 8 from left to right shows the connection between two FreeBOTs. In Fig. 8(a), FreeBOT A and FreeBOT B are not touching each other. Next, FreeBOT A independently rolls to FreeBOT B, as shown in Fig. 8(b). At this time, the internal vehicle of FreeBOT A is at the bottom, so FreeBOT A and FreeBOT B touch each other but are not connected. Following Fig. 8(c) and Fig. 8(d), FreeBOT A's internal vehicle can move toward the contact point between the two FreeBOTs, and FreeBOT A's internal magnet generates strong magnetic attraction to the FreeBOT B's iron shell to achieve the connection between modules. As mentioned above, FreeBOT A's internal magnet will excite a magnetic field in one area, so there is still a connecting force between the modules even if the internal vehicle is not precisely adjusted to the contact point. FreeBOT's connectors are fault-tolerant, just like some advanced MSRR systems. FreeBOT A and FreeBOT B can establish a connection from all directions through the spherical shells, without a complex path planning to align the connector precisely, which to some extent surpasses the existing MSRR system.

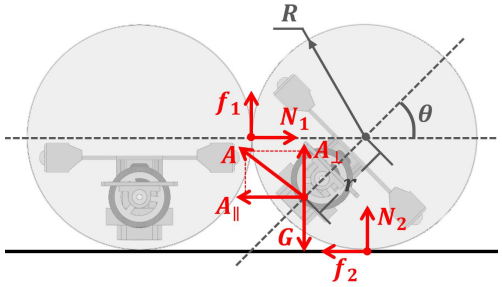

Fig. 9. Force analysis when connecting/separating

Similarly, Fig. 8 shows the separation between FreeBOT A and FreeBOT B from right to left. In Figure 8(d), FreeBOT A's internal magnet is attracting FreeBOT B. Following Fig. 8(b) and Fig. 8(c), the internal vehicle of FreeBOT A gradually moves to the bottom of the spherical shell and the magnetic attraction between FreeBOT A and FreeBOT B gradually weakens. In Fig. 8(b), FreeBOT A and FreeBOT B touch each other but are not connected. Finally, FreeBOT A adjusts the internal vehicle to leave independently as shown in Fig. 8(a). Obviously, the separation between FreeBOTs is the reverse process of the connection.

In conclusion, we only control the position of the internal magnet to realize the connector management of FreeBOT system, without the need for a designated actuator or mechanism to provide this function. However, the connection and separation between FreeBOTs is not feasible on all grounds. If the ground is overly smooth, there is insufficient friction provided to keep the FreeBOT spherical shell still, so the internal vehicle cannot freely adjust its position to connect or separate other FreeBOTs. Next, we analyze the working conditions required of FreeBOT based on Fig. 9. If FreeBOT's shell can maintain the force balance and moment balance, we have

$$\begin{cases} f_1 + A_\perp(\theta) + N_2 = G \\ A_\parallel(\theta) + f_2 = N_1 \\ f_1(R - r\cos\theta) + N_1 r\sin\theta + f_2(R - r\sin\theta) = N_2 r\cos\theta \end{cases}. \tag{5}$$

When the spherical shell is about to slide, f_1 and f_2 can be represented as

$$\begin{cases} f_1 = \mu_1 \cdot N_1 \\ f_2 = \mu_2 \cdot N_2 \end{cases}. \tag{6}$$

Therefore, the required friction coefficient μ_2 can be rep-

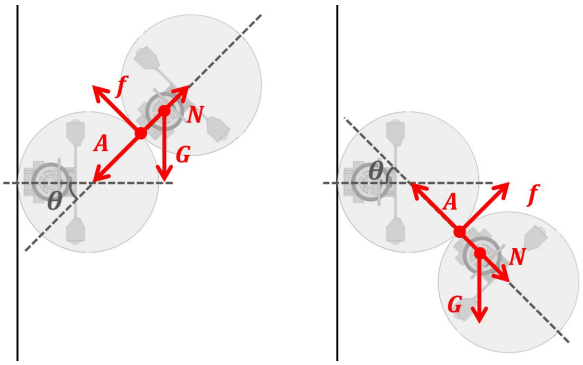

(a) Case on the upper hemisphere (b) Case on the lower hemisphere

Fig. 10. Force analysis of two connected FreeBOTs

resented as the Eq. (7), and the required friction coefficient is different for different lifting angles θ.

$$\mu_2(\theta) = \frac{A_{\parallel}(\theta)(R_2 + \mu_1 R_1 + \mu_1 R_4) + (A_{\perp}(\theta) - G)R_4}{(A_{\perp}(\theta) - G)(R_2 + R_3 + \mu_1 R_1) + \mu_1 A_{\parallel}(\theta)R_3}, \tag{7}$$

where

$$\begin{cases} R_1 = R - r\cos(\theta) \\ R_2 = r\sin(\theta) \\ R_3 = R - r\sin(\theta) \\ R_4 = r\cos(\theta) \end{cases},$$

G is the gravity of FreeBOT, $A(\theta)$ is the magnetic attraction when the angle between the internal magnet and the contact point is θ, R is the radius of FreeBOT spherical shell, r is the distance between the center of gravity and the spherical center, and μ_1 is the friction coefficient between two FreeBOTs. Comprehensively, the two FreeBOT given above parameters can be successfully connected and separated when the friction coefficient between the ground and the FreeBOT is greater than μ_2.

C. Reconfiguration

The combination of multiple FreeBOTs shows some exciting performance. For MSRR system, we are concerned about how to rearrange these modules to different configurations. Different from the previous MSRR system which provides reconfigurable function by specified motor and mechanical design, a FreeBOT can crawl on the surface of other FreeBOT to realize the reconfigurable function. According to the results in Fig. 5, when the internal magnet is slightly raised, the magnetic attraction component in both directions is always positive, which means that will generate a moment force for rolling. Fig. 10 shows two connected FreeBOTs, one of which is connected to a ferromagnetic wall and suspended in the midair. Fig. 10(a) shows two FreeBOTs connected in the upper hemisphere, while Fig. 10(b) shows the case in the lower hemisphere. Next, we analyze the conditions for two FreeBOTs to be connected from multiple angles and maintain static force balance. If the two FreeBOTs in Fig. 10(a) can keep the static force balance, we have:

$$\begin{cases} N = G\sin\theta + A \\ G\cos\theta = f = \mu N \end{cases}. \tag{8}$$

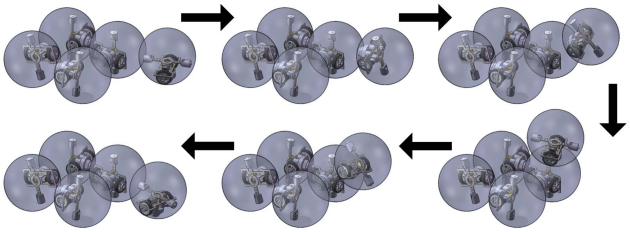

Fig. 11. A simple reconfiguration example of FreeBOT system

So the required friction coefficient under different connection angles can be expressed as

$$\mu(\theta) = \frac{G\cos\theta}{A + G\sin\theta} < \frac{G}{A}. \tag{9}$$

Therefore, we can obtain the connection conditions in the upper hemisphere, that is, the surface friction coefficient required between FreeBOTs are

$$\mu > \frac{G}{A}. \tag{10}$$

Similarly, if the two FreeBOTs in Fig. 10(b) can maintain static balance, then we have

$$\begin{cases} N + G\sin\theta = A \\ G\cos\theta = f = \mu N \end{cases}. \tag{11}$$

So the required friction coefficient under different connection angles can be expressed as

$$\mu(\theta) = \frac{G\cos\theta}{A - G\sin\theta} < \frac{AG\sqrt{\frac{A^2-G^2}{A^2}}}{A^2 - G^2}. \tag{12}$$

Similarly, we can obtain the connection conditions in the lower hemisphere, that is, magnetic attraction A and friction coefficient μ fulfill

$$\begin{cases} A > G \\ \mu > \frac{AG\sqrt{\frac{A^2-G^2}{A^2}}}{A^2-G^2} \end{cases}. \tag{13}$$

Obviously, the conditions in the lower hemisphere are more strict than that in the upper hemisphere. Therefore, as long as the two FreeBOTs can maintain a static connection in the lower hemisphere, connections from all angles are available. (13) is a sufficient condition for two FreeBOTs to be connected from multiple angles and maintain static force balance, that is, FreeBOTs should have a rough shell and strong internal magnets.

FreeBOT can adjust the internal vehicle to connect to another FreeBOT in multi directions. Fig. 11 shows a simple reconfiguration example of FreeBOT system. First, four FreeBOTs are connected to form a robust base. Next, a new FreeBOT independently rolls to and connects to the base. The newly added FreeBOT can change the position of the internal magnet so that the new FreeBOT can be moved to any point on the base surface to rearrange the system into different configurations. Compared with the previous MSRR system, the FreeBOT system has fewer physical constraints in the rearrangement, which means more configurations are available. In general, FreeBOT has greater potential in developing applications for freeform MSRR systems in the future.

TABLE I

SPECIFICATIONS AND PERFORMANCES OF FREEBOT

Specification & Performance	*Value*
Maximum forward Speed	1.2 Body Length/s
Maximum Steering Speed	3.5 rad/s
Time to dock	0.5 seconds
Time to undock	0.5 seconds
Holding force in tension	22.6 N
Wheel Speed (No Load)	60RPM (7.4V)
Wheel Torque	7 kg·cm
Static Module Power Dissipation	0.45 W (7.4V)
Moving Module Power Dissipation	1.38 W (7.4V)
Magnetic remanence	14700 gauss
Magneti size	20×20×10 mm
Overall Dimensions	120×120×120 mm
Module Weight	307.9g

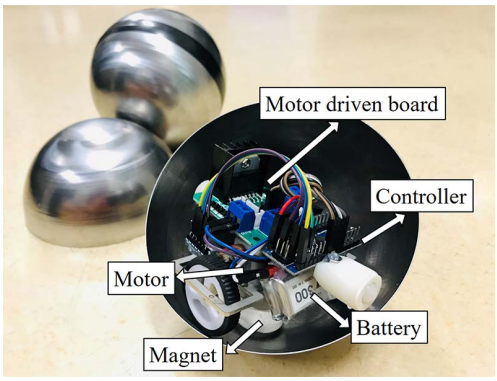

Fig. 12. Prototype of FreeBOT

IV. EXPERIMENTS AND RESULTS

Fig. 12 shows the FreeBOT prototype. Some specifications and performance of FreeBOT are tested, and the detailed information is shown in Table I. Numerous experiments have also been conducted to evaluate the performance of FreeBOT in different aspects, i.e., 1) module independent motion, 2) connection and separation, 3) climbing stairs, and 4) 3D reconstruction. In this paper, FreeBOTs are remotely controlled to show these.

A. Module independent motion

Essentially, as a spherical robot, FreeBOT can realize independent movement on the plane in accordance with the control law of the general spherical robot. In addition, due to the strong internal magnet, FreeBOT can climb up ferromagnetic slopes or even walls. Fig. 13 shows a FreeBOT climbing a ferromagnetic wall. After FreeBOT on the ground adjusts the internal magnet to attract the wall, the FreeBOT can independently move on the wall plane by controlling the internal vehicle.

(a) (b) (c) (d) (e)

Fig. 13. A FreeBOT climbing on the ferromagnetic wall

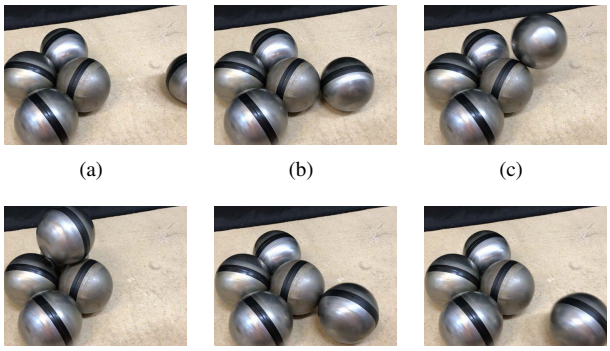

(a) (b) (c) (d) (e) (f)

Fig. 14. Connection and separation between FreeBOTs

B. Connection and separation

Fig. 14 shows the connection and separation between FreeBOTs. Four FreeBOTs are connected together to form a robust base. A new FreeBOT independently comes, and adjusts the internal magnet to connect to the FreeBOT base. Due to the fault-tolerant and freeform connector, the time to dock is only 0.5 seconds (the time to dock is actually the time for the internal vehicle to move from the bottom to the FreeBOT contact point in Fig. 8). After connection, the new FreeBOT can move freely along the surface of the base. Similarly, the time to undock is only 0.5 seconds (the time to undock is actually the time for the internal vehicle in Fig. 8 to move from the FreeBOT contact point to the bottom).

C. Climbing the stairs

Compared with conventional robotic systems, the ability to complete tasks collaboratively is a unique aspect of the MSRR system. Fig. 15 shows two FreeBOTs climbing stairs cooperatively. One FreeBOT cannot climb the stairs independently, but two FreeBOTs can cooperate with each other to achieve this task. The first FreeBOT came to the stairs independently and served as a ladder for the second FreeBOT. Next, the second FreeBOT will connect to the first FreeBOT and adjust the internal magnet to crawl along the surface of the first FreeBOT. Finally, the second FreeBOT separates from the first FreeBOT and comes to the top of the stairs. However, since there is only one FreeBOT as a ladder, it will not be as robust as the base shown in Fig. 14. Therefore, only two FreeBOTs cooperated to climb the stairs are not 100% successful, and the stability will increase if more FreeBOTs join.

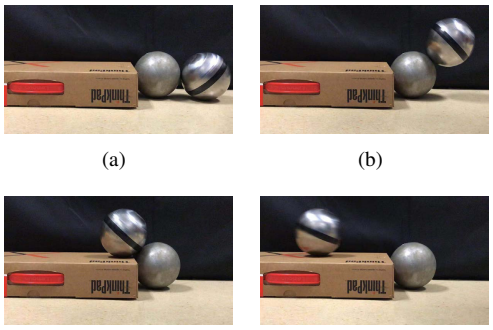

(a) (b) (c) (d)

Fig. 15. Two FreeBOTs climbing the stairs cooperatively

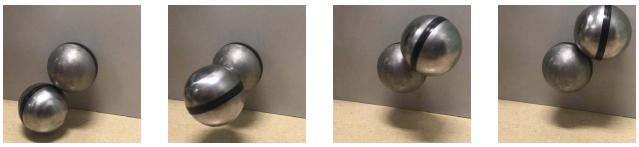

(a) (b) (c) (d)

Fig. 16. Two FreeBOTs show a 3D reconstruction demonstration

D. 3D Reconfiguration

In [2], a SMORES module lifts another module on a plastic structure of passive docking ports to show a demonstration of self-reconfiguration in 3D. We conducted a similar experiment between two FreeBOTs and a ferromagnetic wall (as shown in Fig. 16). A FreeBOT is connected to a ferromagnetic wall and suspended in the air. The tested FreeBOT is connected to the suspended FreeBOT and can be lifted by adjusting the internal magnet. Due to the freeform connector, the tested FreeBOT can be lifted along many paths without constraints, which has great potential for 3D self-reconfiguration.

V. Comparison between FreeBOT and Previous MSRR Systems

FreeBOT has the same basic functions as the most advanced MSRR: module independent motion, connection/separation between modules without manual assistance and system reconfiguration. However, the previous MSRR module is equipped with multiple actuators for different tasks, which increases the weight, volume and manufacturing cost of the robot. FreeBOT has only two motors for these tasks, but it can form an MSRR system with fewer physical constraints. In addition, FreeBOT shows better performance than previous MSRR systems in many aspects, the detailed comparison between these MSRR systems is shown in Table II. But it should be noted that the holding force in tension of FreeBOT is small, which is the weakness of FreeBOT. Although FreeBOT is not competitive in the comparison of holding force in tension, it is sufficient for most tasks.

Multiple MSRR modules forming joints are the main self-reconfiguration method of most MSRR systems. Fig. 17 shows the joint formed by FreeBOT and some previous MSRR system [1], [2], [18]–[20]. In MSRR systems with different architectures, joints composed of modules have different characteristics. The joint composed of the previous MSRR system can only rotate around one axis, while the FreeBOT system can form an unlimited revolute joint. This MSRR self-reconfiguration method with less physical constraints makes the FreeBOT system has great potential to realize freeform robot systems and more applications.

VI. Conclusions and Future Work

This paper proposes a novel MSRR "FreeBOT", which can be connected freely with less physical constraints. FreeBOT only has two motors for multiple tasks: module independent movement, connector management and system reconfiguration. Due to the fault-tolerant and freeform connector, the connection between FreeBOTs is genderless and instant.

TABLE II

Performances of MSRR Modules

Specification	*FreeBOT*	*SMORES*	*ATRON*	*M-TRAN III*	*SuperBot*	*M^3*
No. of DoF	2	4	**1**	2	3	3
No. of Actuators	**2**	5	6	5	9	6
Maximum Connecting No.	**12**	4	8	6	6	3
Ability to Move Independently	**Y**	**Y**	N	N	N	**Y**
No. of Mech. Parts	**24**	132	145	162	-	-
Holding Force in Tension(N)	22.6	60	**800**	25	-	-
Dock Cycle Time (s)	**0.5**	2.3	4	5	50	-
Weight (kg)	**0.31**	0.52	0.83	0.42	1.2	0.8
Data Derived from		[2]	[2], [18]	[1], [2]	[2], [19]	[2], [20]

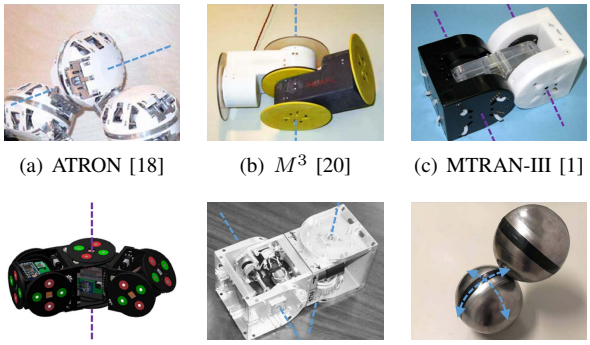

(a) ATRON [18] (b) M^3 [20] (c) MTRAN-III [1]

(d) SMORES [2] (e) SUPERBOT [19] (f) FreeBOT

Fig. 17. Joints consisting of some MSRR systems

Numerous experiments have been conducted to test its performance. The experimental results show that the FreeBOT system has great potential to realize a freeform robotic system.

In this paper, FreeBOT is remotely controlled to demonstrate these experiments. Our group is studying the relative localization [21] and motion planning algorithm [22] for the FreeBOT system. In the future, we will equip FreeBOT with these technologies to realize an autonomous FreeBOT system. In addition, we will increase the number of FreeBOT to fully demonstrate the enormous potential of FreeBOT in realizing more MSRR applications.

References

[1] H. Kurokawa, K. Tomita, A. Kamimura, S. Kokaji, T. Hasuo, and S. Murata, "Distributed self-reconfiguration of m-tran iii modular robotic system," *The International Journal of Robotics Research*, vol. 27, no. 3-4, pp. 373–386, 2008.

[2] J. Davey, N. Kwok, and M. Yim, "Emulating self-reconfigurable robots-design of the smores system," in *IEEE/RSJ International Conference on Intelligent Robots and Systems*, 2012, pp. 4464–4469.

[3] D. Saldana, B. Gabrich, G. Li, M. Yim, and V. Kumar, "Modquad: The flying modular structure that self-assembles in midair," in *IEEE International Conference on Robotics and Automation*, 2018, pp. 691–698.

[4] J. W. Romanishin, K. Gilpin, and D. Rus, "M-blocks: Momentum-driven, magnetic modular robots," in *IEEE/RSJ International Conference on Intelligent Robots and Systems*, 2013, pp. 4288–4295.

[5] A. Sprowitz, S. Pouya, S. Bonardi, J. Van Den Kieboom, R. Möckel, A. Billard, P. Dillenbourg, and A. J. Ijspeert, "Roombots: reconfigurable robots for adaptive furniture," *IEEE Computational Intelligence Magazine*, vol. 5, no. 3, pp. 20–32, 2010.

[6] J. Seo, J. Paik, and M. Yim, "Modular reconfigurable robotics," *Annual Review of Control, Robotics, and Autonomous Systems*, vol. 2, pp. 63–88, 2019.

[7] S. Chennareddy, A. Agrawal, and A. Karuppiah, "Modular self-reconfigurable robotic systems: a survey on hardware architectures," *Journal of Robotics*, 2017.

[8] C. Liu and M. Yim, "Reconfiguration motion planning for variable topology truss." in *IEEE/RSJ International Conference on Intelligent Robots and Systems*, 2019, pp. 1941–1948.

[9] C. Liu, S. Yu, and M. Yim, "A fast configuration space algorithm for variable topology truss modular robots," in *IEEE International Conference on Robotics and Automation*, 2020.
[10] H. Wei, Y. Chen, J. Tan, and T. Wang, "Sambot: A self-assembly modular robot system," *IEEE/ASME Transactions on Mechatronics*, vol. 16, no. 4, pp. 745–757, 2010.
[11] A. Kamimura, H. Kurokawa, E. Yoshida, K. Tomita, S. Kokaji, and S. Murata, "Distributed adaptive locomotion by a modular robotic system, m-tran ii," in *IEEE/RSJ International Conference on Intelligent Robots and Systems*, vol. 3, 2004, pp. 2370–2377.
[12] J. Liedke and H. Wörn, "Cobold-a bonding mechanism for modular self-reconfigurable mobile robots," in *IEEE International Conference on Robotics and Biomimetics*, 2011, pp. 2025–2030.
[13] K. Kotay, D. Rus, M. Vona, and C. McGray, "The self-reconfiguring robotic molecule," in *IEEE International Conference on Robotics and Automation*, vol. 1, 1998, pp. 424–431.
[14] T. Tosun, J. Davey, C. Liu, and M. Yim, "Design and characterization of the ep-face connector," in *IEEE/RSJ International Conference on Intelligent Robots and Systems*, 2016, pp. 45–51.
[15] N. Eckenstein and M. Yim, "Area of acceptance for 3d self-aligning robotic connectors: Concepts, metrics, and designs," in *IEEE International Conference on Robotics and Automation*, 2014, pp. 1227–1233.
[16] J. W. Romanishin, K. Gilpin, S. Claici, and D. Rus, "3d m-blocks: Self-reconfiguring robots capable of locomotion via pivoting in three dimensions," in *IEEE International Conference on Robotics and Automation*, 2015, pp. 1925–1932.
[17] A. Bicchi, A. Balluchi, D. Prattichizzo, and A. Gorelli, "Introducing the" sphericle": an experimental testbed for research and teaching in nonholonomy," in *IEEE International Conference on Robotics and Automation*, vol. 3, 1997, pp. 2620–2625.
[18] M. W. Jorgensen, E. H. Ostergaard, and H. H. Lund, "Modular atron: Modules for a self-reconfigurable robot," in *IEEE/RSJ International Conference on Intelligent Robots and Systems*, vol. 2, 2004, pp. 2068–2073.
[19] B. Salemi, M. Moll, and W.-M. Shen, "Superbot: A deployable, multi-functional, and modular self-reconfigurable robotic system," in *IEEE/RSJ International Conference on Intelligent Robots and Systems*, 2006, pp. 3636–3641.
[20] M. D. Kutzer, M. S. Moses, C. Y. Brown, M. Armand, D. H. Scheidt, and G. S. Chirikjian, "Design of a new independently-mobile reconfigurable modular robot," in *IEEE International Conference on Robotics and Automation*, 2010, pp. 2758–2764.
[21] M. Li, G. Liang, H. Luo, H. Qian, and T. L. Lam, "Robot-to-robot relative pose estimation based on semidefinite relaxation optimization," in *IEEE/RSJ International Conference on Intelligent Robots and Systems*, 2020.
[22] H. Luo, M. Li, G. Liang, H. Qian, and T. L. Lam, "An obstacle-crossing strategy based on the fast self-reconfiguration for modular sphere robots," in *IEEE/RSJ International Conference on Intelligent Robots and Systems*, 2020.